Ordering and metastability in jamming structures of sphere packings

Fan, Wei; Wang, Ju; An, Xizhong; Wu, Yongli; Zou, Yi; Dong, Kejun; Yang, Runyu; Zou, Ruiping; Yu, Aibing

DOI
10.1016/j.partic.2025.02.021

Publication date
2025

Document Version
Final published version

Published in
Particuology

Particuology 99 (2025) 128–139

Contents lists available at ScienceDirect

Particuology

journal homepage: www.elsevier.com/locate/partic

Ordering and metastability in jamming structures of sphere packings

Wei Fan [a, b], Ju Wang [a], Xizhong An [a, *], Yongli Wu [c], Yi Zou [d], Kejun Dong [e], Runyu Yang [f], Ruiping Zou [d], Aibing Yu [d]

[a] Key Laboratory for Ecological Metallurgy of Multimetallic Mineral of Ministry of Education, School of Metallurgy, Northeastern University, Shenyang, 110819, China
[b] Anhui Key Laboratory of Green and Low-Carbon Technology in Cement Manufacturing, Hefei Cement Research & Design Institute Co., Ltd., Hefei, 230051, China
[c] Faculty of Civil Engineering & Geosciences, Delft University Of Technology, 2628, CN Delft, the Netherlands
[d] ARC Research Hub for Smart Process Design and Control, Monash University, Clayton, VIC, 3800, Australia
[e] School of Engineering, Design and Built Environment, Western Sydney University, 2751, Penrith, NSW, Australia
[f] School of Materials Science and Engineering, University of New South Wales, Sydney, 2052, Australia

ARTICLE INFO

Article history:
Received 9 January 2025
Received in revised form
8 February 2025
Accepted 27 February 2025
Available online 7 March 2025

Keywords:
Particle packing
Jamming transition
Ordering and metastability
Dynamics and mechanisms

ABSTRACT

Metastability, disorder and jamming are the typical characteristics of amorphous systems, while the related structure changes remain unclear. Sphere packing is often used as a structure model for amorphous and crystalline states. In this article, sphere packing systems with packing densities ranging from 0.50 to 0.74 were simulated by using Discrete Element Method (DEM), and the obtained packing structures were assessed to investigate the densification process and jamming properties. An order parameter that can effectively distinguish the order and disorder of packing structures was proposed based on the distribution characteristics of jamming angles. Then the evolution of jamming characteristics during the transition from Random Loose Packing (RLP) to Random Close Packing (RCP) and the jamming-jamming relations of different packing structures were demonstrated. On this basis, a correlation between order-jamming-metastable states from the microscopic structural perspective was established, which is of valuable theoretical and practical implications for the characterization and synthesis of crystalline and amorphous materials.

1. Introduction

Comprehending the structural prototype of amorphous materials is pivotal for manipulating their microstructural attributes and decoding the core structural units during phase transition and deformation processes. However, due to the extremely small size of atoms, as well as the randomness of the structure and the complexity of the thermodynamics/kinetics during preparation (Johnson, 1999; Wang, 2012; Zallen, 2008), capturing the atom-level local structure during experiments poses challenges (Miao et al., 2016; Sheng et al., 2006; Yang, 2021), especially *in-situ* monitoring of atomic motion behavior and their interactions (Miyagawa et al., 1988). To address this issue, Bernal and Mason proposed the random packing of spheres to resemble liquids and amorphous materials (Bernal, 1959, 1960; Bernal & Mason, 1960). They achieved a random close packing (RCP) structure by filling mono-sized steel spheres into uneven-walled containers and applying light compression or vibration to minimize the volume occupied by spheres. They also discovered that the radial distribution function (RDF) of a hard sphere packing closely matched that of liquids and amorphous materials, highlighting the high similarity in their structures (Bernal, 1960). The RCP structure can also be realized by numerical models (e.g., Monte Carlo (MC) (Karayiannis & Laso, 2008), molecular dynamics (MD) (Palombo et al., 2013), discrete element method (DEM) (Liu et al., 1999)) to mimic real crystals and amorphous materials at the particulate scale (Bernal, 1960; Bernal & Mason, 1960). Studies have indicated that the transition from the random loose packing (RLP) to RCP can be achieved by applying external energy (e.g., vibration (An et al., 2005; Scott, 1960), light compression (Liu, 2003; Liu et al., 2010)

* Corresponding author.
E-mail address: anxz@mail.neu.edu.cn (X. An).

https://doi.org/10.1016/j.partic.2025.02.021

or air impact (Fan et al., 2022; Gou et al., 2017)). The maximum random packing density of mono-sized hard spheres has been determined from experimental observations as 0.64 (Kamien & Liu, 2007; Yu et al., 2006); this critical value and the formation process show a strong resemblance to the solidification phenomenon of liquids under glass transition(Cohen & Turnbull, 1964).

For the maximum packing density of granular systems, as early as 1611, Kepler conjectured that the densest packing structures for mono-sized hard spheres are hexagonal close-packed (HCP) or face-centered cubic (FCC), with a packing density (or volume fraction Φ) of $\rho = \pi/3\sqrt{2} \approx 0.7405$. This critical value has been mathematically proven (Hales, 2006; Szpiro, 2003). However, a formal mathematical definition or proof for the maximal ρ of an amorphous state (random packing) remains elusive. Based on whether a packing system is jammed and whether it has the minimum order parameters, Torquato et al.(Torquato et al., 2000) proposed a concept of the maximally random jammed (MRJ) state, which not only provides a precise complement to Bernal's definition of RCP, but also reproduces its maximum packing density of $\rho = 0.64$. O'Hern et al. (O'Hern et al., 2003) proposed the jamming-point (J-point) at $\rho = 0.639 \pm 0.001$ for the randomly jammed isotropic packings of spheres in the thermodynamic limit. Parisi et al. (Parisi & Zamponi, 2010) showed that jamming densities are not unique, as those jammed packings may span over the jamming-line (J-line). Recently, Jin et al. (Jin & Yoshino, 2021) extended the jammed states to the jamming-plane (J-plane), showing that the densities of jammed packings are different and protocol-dependent but the J-point is unique with $\rho = 0.655$. Therefore, the densities of critical packing states vary with packing protocols, yet the unique feature of a critical state independent of packing protocols still exists. So it is interesting to further explore the possible unique features underlying the transition from a randomly jammed state to the densest packing state, or from a disordered state to an ordered state. This may help construct a complete phase diagram for jammed hard spheres and precisely delineate their order/disorder characteristics, which has been identified as one of the core challenges in amorphous physics and condensed matter disciplines (Wilken et al., 2021). This requires analyzing different states from an initially random unjamming state to a jamming state and finally an ordered state. In our previous work (An et al., 2005; Liu et al., 1999), packing structures, ranging from RLP to RCP, and to ordered states, were successfully obtained by using different packing protocols (e.g., poured packing and mechanical vibration) based on discrete element method (DEM). Recently, particle packing dynamics under air impact were investigated based on DEM-CFD simulations, where the jamming mechanism due to the structural characteristics was analyzed (Fan et al., 2022). However, a thorough analysis on the general feature/correlation underlying jamming and ordering/disordering states is yet to be conducted.

In this work, various disordered and ordered packing structures of equal spheres with a packing density $\rho \in [0.50, 0.74]$ are generated by DEM and jamming characteristics of particles are analyzed at the particle scale. It elucidates the difference between the disordered and ordered structures and reveals the unique configurations that underpin the stability of RCP. The study further explores the attributes of microscale jamming in order to establish correlations between jamming, structural ordering, and metastable states, based on the intrinsic features within the dynamics and stability of a particle system.

Table 1
Parameters used in the simulation for ordered packings ($\rho = 0.64$–0.74).

Parameters	Values
Particle diameter (mm)	5
Particle density (kg/m^3)	2500
Young's modulus (Pa)	1×10^9
Gravitational acceleration (m/s^2)	9.81
Poisson's ratio	0.29
Coefficient of restitution	0.3
Coefficient of sliding friction	0
Coefficient of rolling friction	0
Batch (particles/s)	500
DEM time step (s)	5×10^{-6}
Particle velocity (m/s)	0–70

2. Simulation method and conditions

2.1. Governing equations and numerical issues

In the DEM model (Liu et al., 1999), the granular material is treated as an assembly of discrete particles. The motion of each particle is governed by Newton's second law:

$$m_i \frac{\mathrm{d}\vec{v}_i}{\mathrm{d}t} = m_i \vec{g} + \sum_{j=1} \left(\vec{F}^{\mathrm{n}}_{ij} + \vec{F}^{\mathrm{s}}_{ij} \right) \tag{1}$$

$$I_i \frac{\mathrm{d}\vec{\omega}_i}{\mathrm{d}t} = \sum_{j=1} \vec{R}_i \times \vec{F}^{\mathrm{s}}_{ij} - \mu_{\mathrm{r}} \vec{R}_i \left| \vec{F}^{\mathrm{n}}_{ij} \right| \vec{\omega}_i \tag{2}$$

where m_i, $\vec{v}_i$, $\vec{\omega}_i$ and I_i are the mass, translational velocity, angular velocity, and moment of inertia of particle i, respectively; $\vec{R}_i$ is a vector running from the center of particle i to the contact point; and μ_{r} is the coefficient of rolling friction. $\vec{F}^{\mathrm{n}}_{ij}$ and $\vec{F}^{\mathrm{s}}_{ij}$ denote the normal contact force and tangential contact force imposed on particle i by particle j, given by:

$$\vec{F}^{\mathrm{n}}_{ij} = \frac{4}{3} E' R'^{1/2} \delta_{\mathrm{n}}^{3/2} - 2 \frac{\ln e}{\sqrt{\ln^2 e + \pi^2}} \sqrt{\frac{5}{3} m' E' R'^{1/2}} \delta_{\mathrm{n}}^{1/4} \vec{v}^{\mathrm{rel}}_{\mathrm{n}} \tag{3}$$

$$\vec{F}^{\mathrm{s}}_{ij} = \begin{cases} 8G' R'^{1/2} \delta_{\mathrm{n}}^{1/2} \delta_{\mathrm{t}} - 2\sqrt{\frac{5}{6}} \frac{\ln e}{\sqrt{\ln^2 e + \pi^2}} \sqrt{8G' R'^{1/2} \delta_{\mathrm{n}}^{1/2} m'} \vec{v}^{\mathrm{rel}}_{\mathrm{t}} & \text{if } \left| \vec{F}^{\mathrm{s}}_{ij} \right| \le \mu_s \left| \vec{F}^{\mathrm{n}}_{ij} \right| \\ -\mu_s \vec{F}^{\mathrm{n}}_{ij} & \text{if } \left| \vec{F}^{\mathrm{s}}_{ij} \right| > \mu_s \left| \vec{F}^{\mathrm{n}}_{ij} \right| \end{cases} \tag{4}$$

where E', R', and m' are the equivalent Young's modulus, the equivalent radius and the equivalent mass, respectively; δ_n

Table 2
Parameters used in the simulation for amorphous packings ($\rho = 0.5–0.64$).

Parameters	Values
Particle diameter (mm)	5
Particle density (kg/m^3)	2500
Young's modulus (Pa)	1×10^9
Gravitational acceleration (m/s^2)	9.81
Poisson's ratio	0.29
Coefficient of restitution	0.3
Coefficient of sliding friction	0, 0.05, 0.1, …, 1
Coefficient of rolling friction	0, 0.05, 0.1, …, 1
DEM time step (s)	5×10^{-6}
Particle velocity (m/s)	0

represents the normal overlap; $\vec{v}_n^{rel}$ is the relative normal velocity; e represents the restitution coefficient; μ_s is the coefficient of sliding friction; $\vec{v}_t^{rel}$ represents the relative tangential velocity; and G' is the equivalent shear modulus.

2.2. Methodology for structure constructions

Various packing structures of equal spheres with densities between 0.50 and 0.74 were numerically reproduced by DEM. Tables 1 and 2 lists the key parameters of the simulation. Firstly, spheres with diameter d of 5 mm were generated in a $20d \times 20d \times 60d$ container under gravity, forming random packing structures with ρ ranging from 0.50 to 0.64 by adjusting the friction coefficient of the particles. Specifically, the packing density obtained from frictionless particles was 0.64 (Finney, 1970; Lubachevsky & Stillinger, 1990; Mueth et al., 1998). A previous study demonstrated that the formation of ordered packing structure is facilitated by reducing particle deceleration and increasing interparticle collisions (Lubachevsky & Stillinger, 1990), where the MD method was used to assign initial velocities to the particles and to compress the space in which the particles are located. The lower the compression velocity, the more the particles collide, and the easier it is for them to form ordered structures, i.e., the slower dynamics allow the formation of crystals from multiple collisions. In this study, the frictionless particles were given different initial velocities so that they had different numbers of collisions and thus formed packing structures with different densities. Therefore, an initial velocity was introduced to the frictionless hard spheres. By varying the velocity and allowing the particles to undergo a gradual dissipation of energy, different ordered packing structures with $\rho \in [0.64, 0.74]$ were generated. The evolution of the packing density ρ with initial velocity as shown in Fig. 1 demonstrates that ρ is greatly improved with increasing velocity (i.e., increasing number of collisions), and when ρ approaches 0.74, the particle system has reached a very dense packing state and its density no longer varies significantly with increasing velocity. Different random packing structures were obtained by controlling the friction coefficient of the particles with no initial velocity, and the results are shown in the inset of Fig. 1, from the figure one can find that ρ decreases dramatically with the friction coefficient, where ρ of the frictionless particles is approximately 0.64, which corresponds to the packing density of the RCP structure. Note that the periodic boundary conditions (PBC) were imposed in the horizontal direction to eliminate the boundary effect. In addition, the particles within $4d$ from the top and bottom surfaces were not included in the calculation of packing density.

3. Result and discussion

3.1. Jamming properties

Previous studies have made classifications on the jammed and free states of particles in a packing (Torquato et al., 2000). Specifically, a particle is in a jammed state if it cannot be freely moved while all other particles are fixed in the system; otherwise, it is regarded as in a free state. Fig. 2 lists the achievable jammed packing structures related to the order parameter (the gray region is inaccessible), in which the RCP state is better defined as the maximally random jammed, namely, the state with the minimized order parameter among all statistically homogeneous and isotropic jammed structures. In our previous work (Fan et al., 2022), a similar approach was also used to analyze the obstructiveness of packings. Specifically, a particle is free if there is no contacting particle in front of it (i.e., in the plane perpendicular to its motion direction), otherwise it is defined as jammed. By analyzing the obstructiveness of particle motion in a granular system under air impact, it was found that almost no particles in the packing can move freely when ρ reaches 0.64 (according to the free volume theory, the absence of available free volume within the packing hinders the motion of particles; therefore, there is free volume near particles that can move unobstructed, which can be called free particles). However, the previous analysis only considered the jamming of dynamic packings. This study further investigates the jamming of potential particle motion in static packings based on the following three possible directions of particle motion:

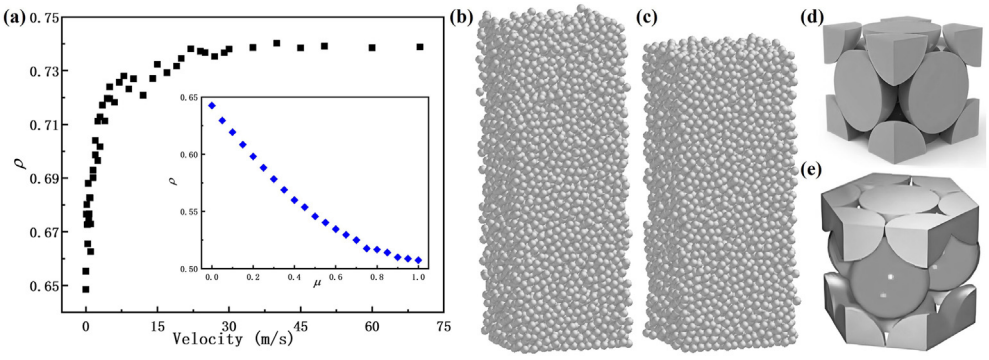

Fig. 1. (a) The relationship between packing density and velocity when $\mu = 0$, where the inset figure shows the relationship between packing density and friction coefficient of particles when $V = 0$ m/s. Note, although PBC is used, the Voronoi tessellation still leaves relatively large cell volumes for boundary particles, so particles within $2d$ of the boundary in the horizontal direction were excluded for all following analyses. (b) Random loose packing. (c) Random close packing. (d) Face centered cubic unit cell structure. (e) Hexagonal close packed unit cell structure.

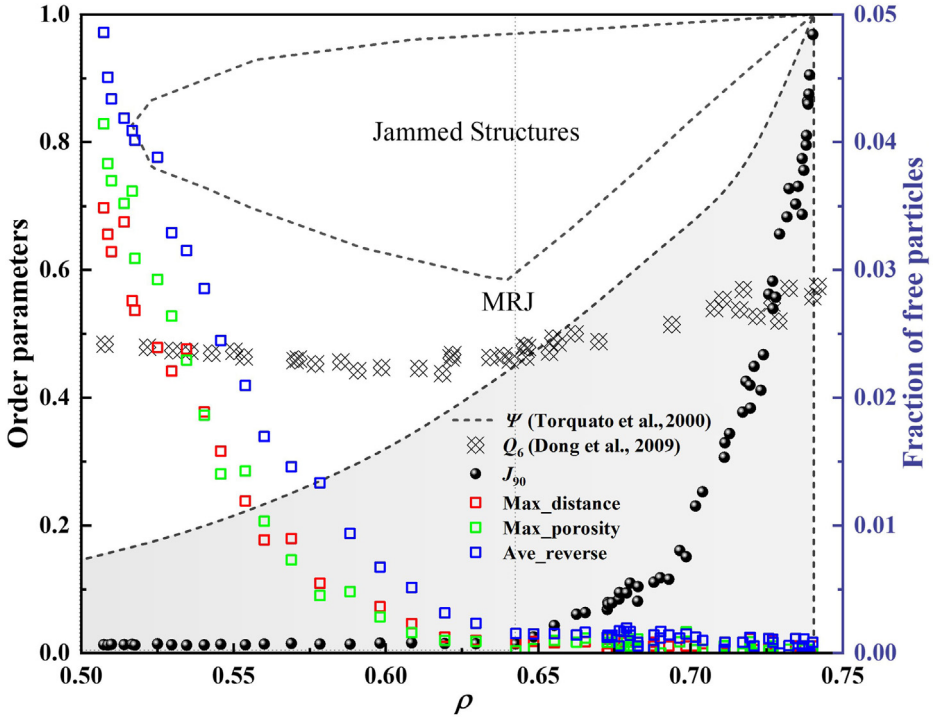

Fig. 2. Correlations between order parameters and the fraction of free particles with packing density.

- The direction of the maximum nearest neighbor distance, i.e., the direction of the longest $\overrightarrow{ij}$, where $\overrightarrow{ij}$ represents the vector between particle i and its neighboring particle j (Fan et al., 2022)
- The direction of maximum porosity, i.e., the direction in which the particle points to the center of its neighboring tetrahedron with the largest <p> (here, <p> is the local porosity of the neighboring tetrahedron) (Fan et al., 2022).
- The average opposite direction of contacts, i.e., the opposite direction of the sum vector of all contacts $\overrightarrow{ij}$. For a particle, if there is a contact in a certain direction, moving away from that direction is most likely for it to move freely. Therefore, the average opposite direction of contacts represents the direction in which the particle is most likely to be unobstructed.

By analyzing the obstructiveness of particle motion in the three directions in various packing structures, we obtained similar results: the proportion of free particles decreases with increasing packing density; at $\rho = 0.64$, the proportion of free particles in the granular system is almost negligible. This microscopic analysis supports the existence of the jamming-point at $\rho = 0.64$.

It is evident that the value of each order parameter associated with the MRJ state is not zero. While the values of the commonly used order parameters in a non-jammed packing system are high, such as bond orientation order Q_6 (Dong et al., 2009; Steinhardt et al., 1983), tetrahedral order (Anikeenko & Medvedev, 2007), structural order (Tong & Tanaka, 2018, 2019), multi-tetrahedral order (Nelson & Spaepen, 1989) and anisotropy indicators(Schröder-Turk et al., 2010), these parameters still exist and vary with packing density even though its value is lower than 0.64. Theoretically, an order parameter is expected to be close to zero for all random systems with $\rho = 0.50–0.64$ and a superlinear growth from $\rho = 0.64$ to 0.74. In this work, we propose an order parameter, J_{90} (the proportion of 90° jamming angles in all jamming angles other than 60°; its comprehensive description will be detailed in subsequent section), which can more closely match the theoretical expectation, as shown in Fig. 2. It is worth noting that in the previous work (Fan et al., 2022), the total proportion of HCP and FCC local clusters shows similar results to J_{90} (Amirifar et al., 2018, 2021). However, the demonstration of order by the proportion of a particular structure rather than by a specific structural feature undoubtedly lacks universality.

3.2. Order properties

Inspired by the above jamming analysis and molecular bond angles (Hoy, 2017), we proposed the concept of the jamming angle (defined as the angle between two neighboring contact vectors, similar to molecular bond angles) to elucidate the microscopic properties of packing structures. The calculation of the jamming angle is shown in Fig. 3(a). First, the neighboring particles of a given particle (particle i) are obtained by the Voronoi tessellation (Bernal, 1959). Then, the contact of particle i with a neighboring particle is determined if the distance between their centers is less than or equal to $1.005d$. For contacting particles, their jamming angle is calculated. Note that if there are additional contact vectors between two given contact vectors, their neighboring relationship is ignored and their jamming angle is not calculated. In the local structures shown in Fig. 3(a), the third case does not have a jamming angle of 120° because it contains six individual 60° jamming angles. The fourth structure, on the other hand, has a 120° jamming angle since no other contact vectors are between the two 120° angular contact vectors.

After all the jamming angles are calculated, their distributions are obtained as shown in Fig. 3(b), where $f(\theta)$ represents the probability of finding jamming angles within a ±0.5° range around angle θ. For example, $f(60)$ denotes the probability of finding jamming angles in the range 59.5–60.5°. Fig. 3(b) indicates that for each packing structure, the distribution curve of $f(\theta)$ has three evident peaks, i.e., 60°, 90°, and 120°. Furthermore, the values of

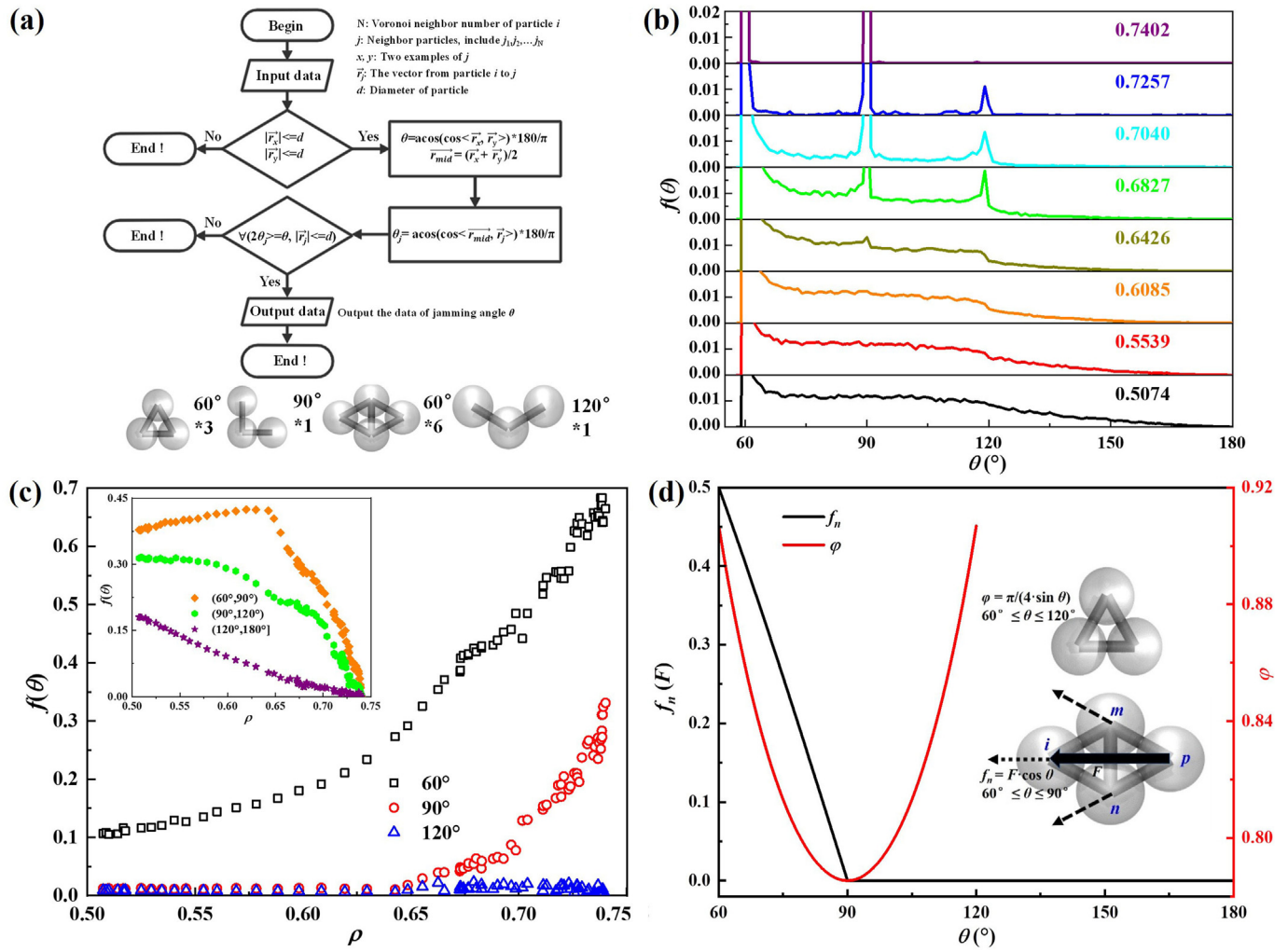

Fig. 3. (a) Flowchart of jamming angle calculation and some typical jamming angles (inset). (b) Relationship between $f(\theta)$ and θ for different packings. (c) Relationship between $f(\theta)$ and ρ for different jamming angles. (d) Properties of different jamming angles, showing the mechanical stability of local structures at different jamming angles and the local volume fraction; here, a particle is introduced to fill the jamming structure of particle i with a force F that points to the center of the three particles forming the jamming angle. The force on particle i that can be withstood by the structure is considered as the mechanical stability of the structure, i.e., a higher force corresponds to a better mechanical stability.

other $f(\theta)$ show a decreasing trend as the angle increases. Statistical analysis of the peak values of the angle distributions and the jamming angles between the peaks yield the relationship between $f(\theta)$ and ρ for several characteristic angles. As indicated in Fig. 3(c), the peak at 60° is prevalent in all packing structures and shows a superlinear growth with ρ. The peak at 90° only appears when $\rho > 0.64$ and also follows a superlinear growth with ρ. The peak at 120°, on the other hand, is relatively low and appears only when $\rho > 0.64$, with little variation as ρ changes. In a 2D packing of circles or disks, the equilateral triangle configuration is the most compact local structure, while in a 3D packing of spheres, the tetrahedral configuration is the most compact local structure. However, unlike the equilateral triangle, a dimer or wagon wheel structure composed of gapless tetrahedra is constrained by their quantity (Zhao et al., 2019), making complete spatial filling unattainable. To promote a higher number of tetrahedral configurations within a given space, gaps are unavoidable (Aste & Weaire, 2000), which results in a jamming angle exceeding 60° between spheres. For instance, it is known that the ordered FCC or HCP structure formed by equal hard spheres has the maximum packing density and the highest number of tetrahedral configurations, which manifest 24 jamming angles at 60° and 12 jamming angles at 90° within a unit cell (as shown in Fig. 1(d) and (e)). Therefore, the emergence of jamming angles at 90° may correspond to the signature of structural transition towards an ordered and dense packing ($\rho > 0.64$). Accordingly, the jamming angle parameter may reveal the ordered nature of a microscopic jamming structure in a sphere packing system, which provides a better and more complete index than using the ratio of HCP and FCC structures in characterizing ordering characteristics in granular matter.

For spheres in random packings, the regular tetrahedral structure (i.e., $\theta = 60°$) is more stable than the formation of the structure with $\theta = 90°$.Fig. 3(d) shows the mechanical stability and packing density of local jamming structures ranging from 60° to 180°, where the mechanical stability refers to the ability of a local jamming structure to withstand external forces. To calculate the mechanical stability, a jamming structure with an angle of θ formed by three particles (e.g., particles i, m, and n) is firstly constructed. Then particle p is introduced to fill the jamming structure around particle i under a driving force F which points to the center of the three particles that form the jamming angle. In the filling process, particles m and n are subject to forces that push them apart in opposite directions. In this case, if particle i remains stationary, the structure is susceptible to damage as particles m and n are separated.

However, if the three particles shift to the left as a whole, the force F cannot fully act on the local structure to cause damage, and then the mechanical structure is stable. Therefore, the force f_n acting on particle i (which represents the ability of particle i to deviate from the force F and is also the total force exerted by particles m and n on particle i) is used to reflect the mechanical stability of the local jamming structure. It is found that f_n decreases with angle θ (proportional to the cosine of the angle) and becomes 0 at $\theta = 90°$, and the local packing density is also at its minimum at 90°. Obviously, the occurrence of many jamming structures at exactly 90° is really difficult.

As a result, based on the fact that more 60° jamming angles and fewer 90° jamming angles exist in a random packing system, it can be concluded that the 60° jamming represents the locally densest structure that commonly exists in both ordered and random packings, while the 90° jamming is more typical in the ordered packings and is replacing the 60° jamming when a jammed packing experiences order transition. Therefore, we define J_{90} (where $J_\theta = f(\theta)/(1\text{-}f(60))$) as an order parameter, which quantifies the gap characteristic for the maximum existence of ordered structures as an indicator of ordering. As shown in Fig. 2, this order parameter can effectively meet the requirements of an ideal order parameter: (1) The index is 0 for random systems; and (2) it starts to increase from a certain density inflection point and reaches 1 for a completely ordered structure. The calculation of this index is based on the 90° gap characteristic of HCP/FCC structures and remains valid for the simple cubic (SC) structure. For the body-centered cubic (BCC) structure with only two characteristic jamming angles (70.5° and 109.5°), $J_{70.5}+J_{109.5}$ is used as a metric to evaluate its degree of ordering, which can discriminate ordered and random features. In summary, we use the locally densest structure widely existing in amorphous states as a reference, and compare it with other specific angular distribution $f(\theta)$ corresponding to the significant occurrence of the densest structures as a measure of ordering. This method can also be extended to polycrystalline structures.

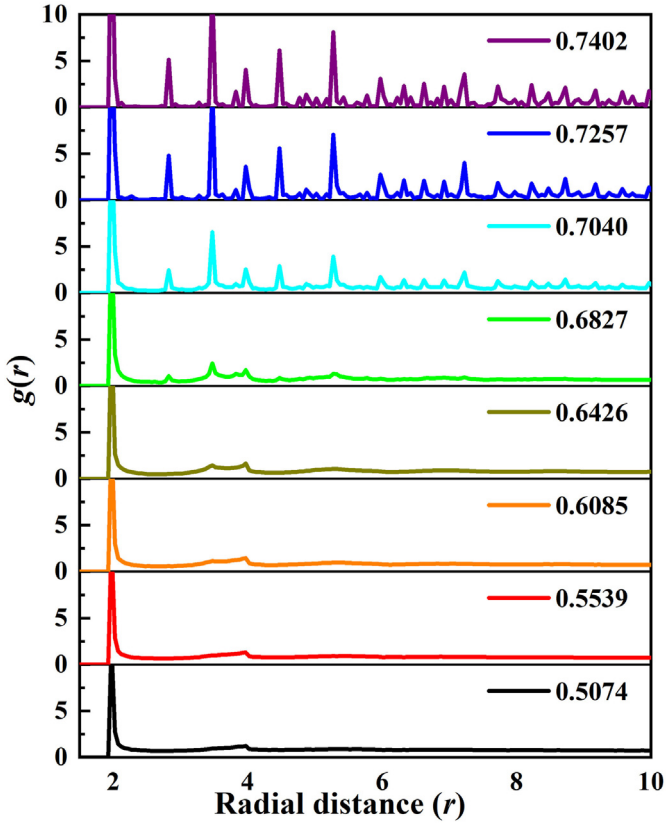

Fig. 4. Radial distribution functions of different packing structures.

The radial distribution function is a common method for characterizing the crystal packing structure (Mueth et al., 1998), which is defined as the probability of finding a particle center at a given distance from a given particle center, calculated by $g(r) = \frac{1}{Nn_0\pi r}\sum_{i=1}^{N}\sum_{j=i+1}^{N}\delta(r_{ij} - r)$, where n_0 is the average particle density, N is the total number of particles, r_{ij} is the distance between particles i and j, and δ is the Dirac function with $\delta(0) = 1$. Previous investigations have identified three distinct peaks in the RCP (Finney, 1970), i.e., the first at $2r$, the second at $2\sqrt{3}\,r$, and the third at $4r$. The RDF of different packing structures (Fig. 4) indicates that as ρ increases from 0.50 to 0.64, g(r) gradually shows a split-second peak at $2\sqrt{3}\,r$, which is a typical feature of the RCP structure. For the particle system with $\rho > 0.64$, the RDF curves of all four packing structures have many isolated peaks, indicating that there is a long-range correlation between the positions of the particles in the final packing, which is a typical feature of ordered packing. It is worth noting that, as seen in the figure, after $\rho > 0.64$ a new peak appears in the RDF curve at $2\sqrt{2}\,r$ between $2r$ and $2\sqrt{3}\,r$. This corresponds to the 90° jamming structure mentioned above, and this is the reason why we use J_{90} as the order parameter. Of course, one can use the evolution of this peak as a characterization of the order of the packing structure, but it is less computationally simple than J_{90} in terms of ease of calculation and therefore will not be further discussed.

The contact angle distribution is another way to characterize the structural properties of particle packing. Here, the contact angle refers to the orientation of the normalized contact force, which is defined as the acute angle between the contact vector and the vertical direction, and the orientation characteristics of its distribution can reflect the anisotropic or isotropic nature of the granular material. Fig. 5(a)–(c) shows the contact angle probability distribution function (PDF) in different packings, and (d)-(f) are the distributions of the normalized normal force $f(a)$ for different angles (see Ref (Fan et al., 2022). for the definition of $f(a)$). For the packing structures with $\rho \leq 0.64$, the distributions of different angles are generally uniform and the magnitude of each orientation force is almost the same. For the packing structures with $\rho > 0.64$, the angular distribution curves show very high peaks at 90° and 35°, and their $f(a)$ also shows obvious peaks at 90°, 35° and other angular positions, indicating the anisotropy of these packing structures.

3.3. Metastable properties

Previous studies based on mean-field theory indicated that the crucial feature of disordered systems is the vast majority of metastable states (Parisi et al., 2020), and a bifurcation occurs in the phase diagram of a hard sphere packing system around a packing density of 0.50, with one branch representing the crystalline transformation towards the FCC or HCP structure and the other branch representing the metastable amorphous realization towards the RCP structure (Parisi & Zamponi, 2010). Therefore, the relationship of the metastable amorphous state and stable crystalline state is incompatible, e.g., for a jamming system, an increase in one state inevitably leads to the decrease in the other state. For a non-jamming system such as a simple liquid or a supercooled liquid, its transition to the glass (amorphous) state induces an increase in the metastable state. By analyzing the structural peaks, we find that prior to the jamming point ($\rho = 0.64$), the $f(\theta)$ increases

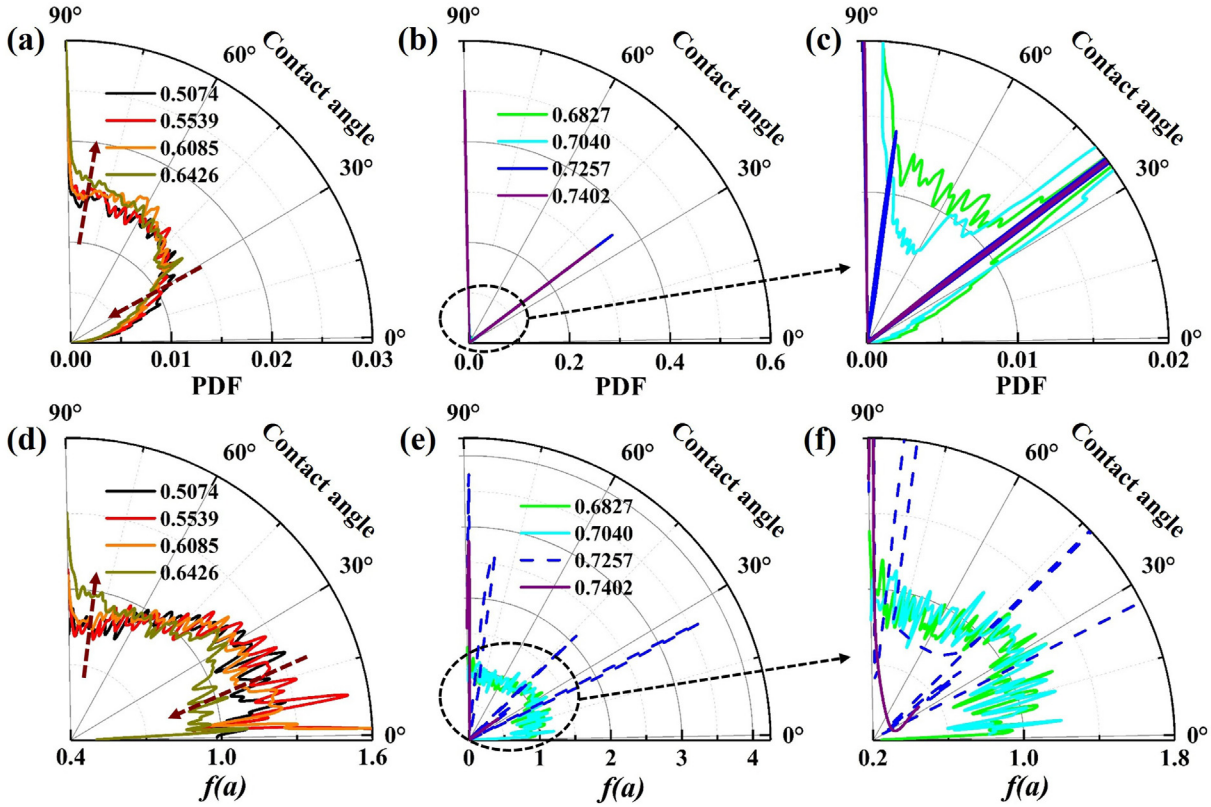

Fig. 5. Contact angle distributions (a)–(c) and normalized contact normal forces along angles between particles (d)–(f) in different packings.

with ρ within the (60°, 90°) jamming. However, beyond the jamming point, there is a significant decrease in $f(\theta)$ with ρ, which shows an opposite trend to the 90° jamming, as shown in Fig. 3(b) and (c). Since the amorphous state cannot transit to the crystalline state by a continuous increase in packing density, the figure can be interpreted from right to left after $\rho = 0.64$, implying that the continuous disruption of the crystalline structure leads to the reduction in packing density. Remarkably, this perturbation is accompanied by a significant decrease in 90° jamming and a substantial increase in (60°, 90°) jamming. The characteristics of (60°, 90°) jamming are consistent with the definition of metastable states (Binder, 1987) and show an agreement with previous descriptions of metastable structural configurations (Lohr et al., 2010). Based on these findings, we define (60°, 90°) jamming as metastable jamming. The occurrence of metastable states is directly correlated with the dynamical slowdown of the liquid; i.e., there is a significant dynamical slowdown of the atomic motion in the liquid under supercooled conditions (Tong & Tanaka, 2019), and the local pursuit of the densest packing structure to form 60° jamming and the formation of 90° jamming without sufficient nucleation time are contradicted. Therefore, the formation of metastable jamming structures between 60° and 90° to maintain structural stability is an inevitable consequence.

In the previous work (Fan et al., 2022), it was observed that the transition of mono-sized sphere packings from RLP to RCP can be achieved by air impact. This transition is accompanied by the evolution of contact structures, where the specific oriented normal forces lead to the "freezing" phenomenon when reaching the densest amorphous state, resulting in the overall jamming of the packing system. In this work, it is found that microstructural jamming is composed of two contact vectors $\overrightarrow{im}$ and $\overrightarrow{in}$. These vectors undergo five different evolutions in the air impact process: (1) "Disappear"-both contact vectors forming the jamming angle disappear after the impact; (2) "Add"-two new contact vectors appear and form a jamming angle after the impact; (3) "Change"-both contact vectors remain after the impact and maintain the jamming angle; (4) "Fill"-both contact vectors remain after air impact, but no longer form the jamming angle because of other contact vectors in between; (5) "Replace"-one contact vector remains while the other is replaced by a new vector after the impact, resulting in the formation of a new jamming angle. As shown in Fig. 6, regardless of the evolution modes, the resulting jammed structures are predominantly characterized by (60°, 90°) jamming angles, while the characteristic angles associated with the ordered jamming hardly participate in the evolution process. This phenomenon is particularly evident in cases of "change" and "fill", indicating the predominant effect of the (60°, 90°) metastable jamming structures in a random packing system. Fig. 7 shows the evolution of jamming angles in the packing after densification from $\rho = 0.60$ to $\rho = 0.61$ under air impact. The evolution phenomenon mentioned in Fig. 6 (regardless of the method of evolution, the final jamming structure is dominated by (60°, 90°) jamming, and the characteristic angle of the ordered jamming is hardly involved in the evolution of the structure) becomes more obvious with the subdivision of the stages, which confirms the predominant effect of the (60°, 90°) metastable jamming structures.

In the simulation, the formation of the structure occurs first at the bottom of the vessel. In the previous section it was mentioned that the phase diagram for jammed hard spheres has both ordered and metastable branches, which are mutually exclusive. In other words, an increase in the number of one feature is accompanied by a decrease in the other. Since a random structure cannot be

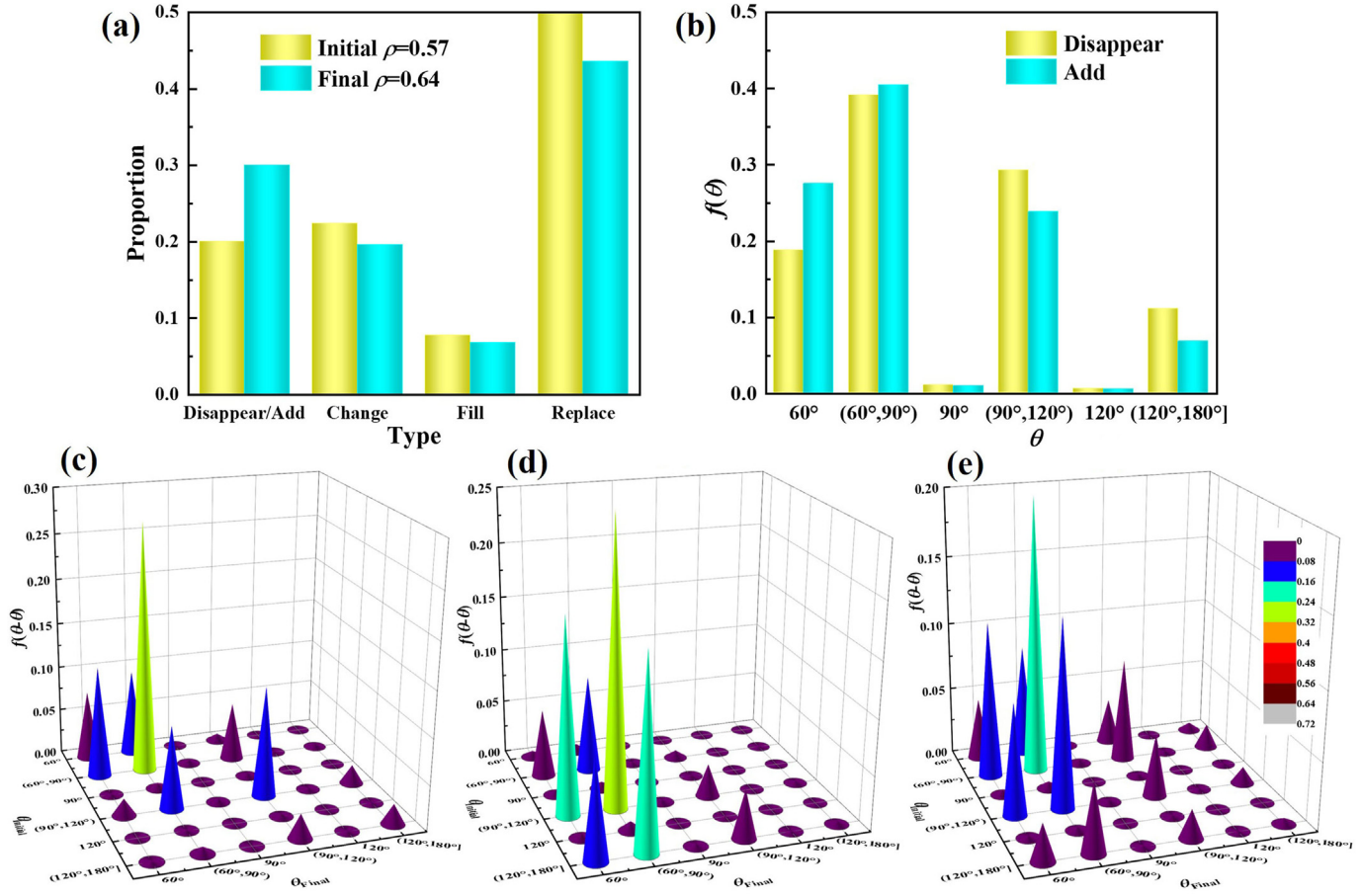

Fig. 6. Evolution of jamming angles in the packings after densification from $\rho = 0.57$ to $\rho = 0.64$ under air impact, where: (a) proportion of different evolution types; (b)–(e) probability of jamming angles in the evolution types of "Disappear/Add", "Change", "Fill", and "Replace". Note: the packing structure with an initial ρ of 0.57 increases to 0.64 after air impact. For the jamming angle, if the two vectors $\overrightarrow{im}$ and $\overrightarrow{in}$ that form the jamming angle both disappear in the final structure, then the evolution type of the jamming angles is "Disappear"; if there are two new vectors forming the jamming angle in the final packing, the evolution type is "Add"; if the two vectors still exist and form jamming angle, then the evolution type is "Change"; if the two vectors still exist, but no longer form a jamming angle, indicating that particles have filled the previous jamming structure, and this evolution type is "Fill"; if only one of the two vectors remains while the other is replaced by a different vector to form a jamming angle, this evolution type is termed as "Replace".

transformed into an ordered structure by successive density changes, it is assumed that the destruction of an ordered system is accompanied by a significant decrease in the ordered features and an obvious increase in the metastable features. From Fig. 8 one can find that for both random and densest ordered packings, the distributions of different jamming angles in the axial direction are uniform. For locally ordered packing structures (e.g., $\rho = 0.6827$ and $\rho = 0.7257$), it can be seen that the local ordering structure is mainly near the bottom of the vessel, and as the packing structure is formed layer by layer, the transition zone from ordered to RCP packing shows a decrease in the ordered jamming angle and an increase in the metastable jamming angle and other jamming angles. Combined with figures above, we believe that the inability of RCP to achieve further densification while remaining stable is related to the (60°, 90°) metastable jamming structure.

To further investigate the correlation between jamming, order and metastable properties of packings, we analyze the so-called jamming-jamming relationship which is the jamming angle and its correlation of particle filling a jamming structure around it. The calculation procedure is as follows: 1) for a given jamming angle in a packing structure, we search the particle p that is closest to the midpoint between particles m and n; 2) assign particle p a motion vector pointing toward the midpoint to simulate the tendency of particle p to fill the jamming structure (as shown in Fig. 3(d)) (note that this step only involves assigning a motion vector to particle p for the purpose of calculating the motion jamming angle, no actual movement of the particle occurs); 3) if particle p encounters any other particles in its forward motion (within a 90° spatial range relative to the motion direction), the smallest angle between the motion vector and each contact vector will be calculated; this smallest angle is multiplied by 2 to define θ_2 (motion jamming angle), and the jamming angle filled by particle p is regarded as θ_1 (filled jamming angle). If there are no particles in contact within a range of 90° in the motion direction of particle p, motion jamming angle is 180°; 4) after calculating motion jamming angle for each filled jamming angle, the jamming-jamming relation between the filled jamming angle and the motion jamming angle is then established.

The probabilities of 36 typical jamming-jamming relations in different packings are shown in Fig. 9(a)–(e). For all the packing structures, the jamming-jamming relations are mainly concentrated within the same type with fewer cases for cross-type relations, and the occurrence of cross-type relationships decreases with increasing ρ. After ρ reaches 0.64, only the cross-type relationships between (60°, 90°) and (90°, 120°) remain, and their peaks are almost identical. For the densest structure, there are no cross-type relationships and only two peaks of 60°–60° (the jamming-jamming relationship between 60° and 60°) and

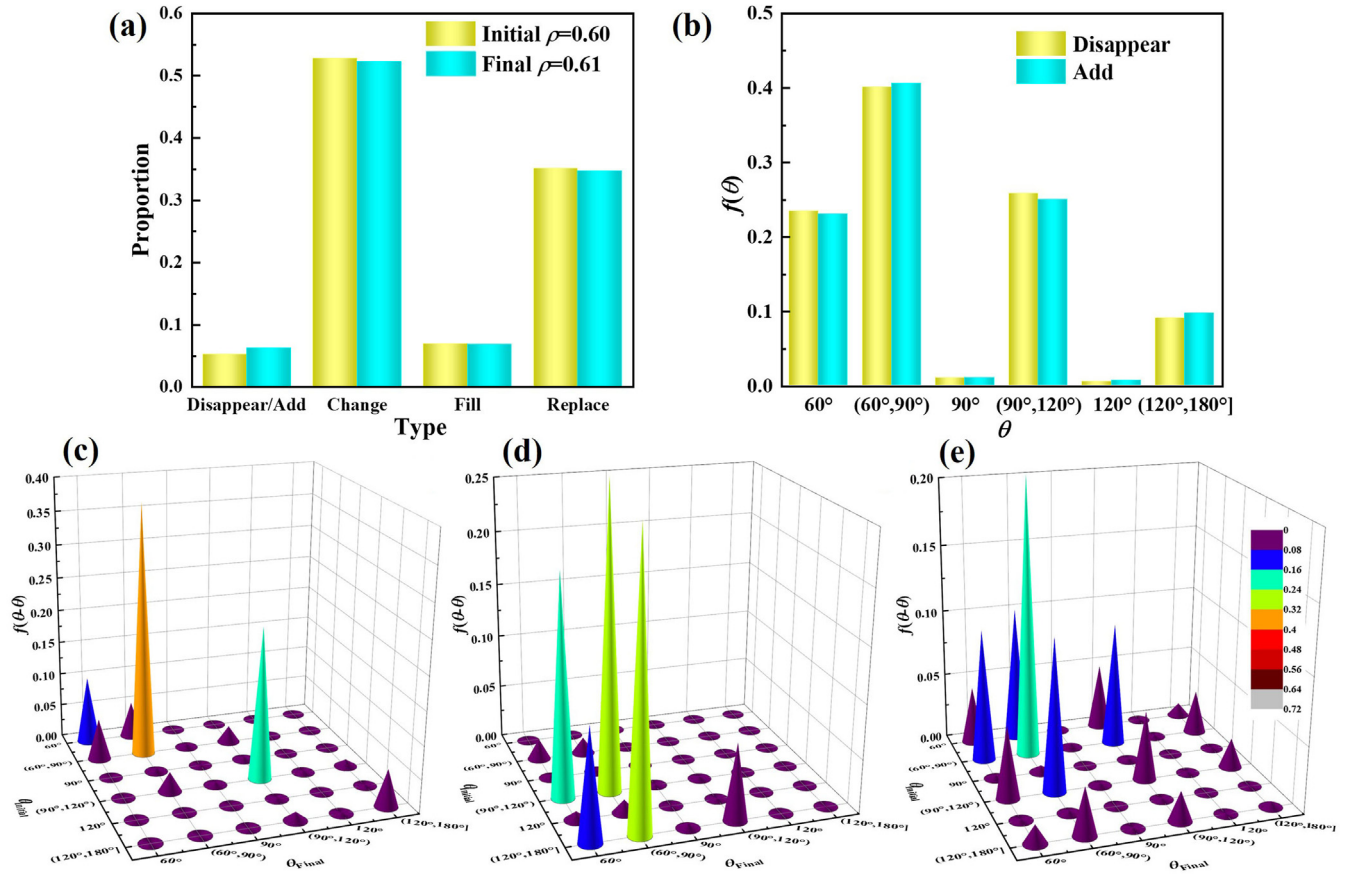

Fig. 7. Evolution of jamming angles during densification from $\rho = 0.60$ to $\rho = 0.61$ under air impact, where: (a) ratio of different evolution types; (b)–(e) probability of jamming angles in the evolution types of "Disappear/Add", "Change", "Fill", "Replace".

90°–90°. Since the motion jamming angle for the jamming system is based on the minimum angle, it should be less than or equal to that of the filled jamming angle. However, the variation of the mean jamming angles with ρ as shown in Fig. 9(f) indicates that, for packing structures with $\rho < 0.64$, motion jamming angle is larger than filled jamming angle, implying the presence of a large amount of free volume in the structure. With $\rho \geq 0.64$, the mean values of filled jamming angle and motion jamming angle are nearly identical, indicating the "freezing" of the free volume (Cohen & Turnbull, 1964), confirming the critical jamming point at 0.64 (Jin & Yoshino, 2021). In addition, for a packing with $\rho < 0.64$, there are no occurrences of 90° and 120° in motion jamming angle. The highest peak corresponds to the metastable jamming peak at (60°, 90°), which increases with ρ. However, for $\rho \geq 0.64$, the metastable jamming peak (60°, 90°) decreases, accompanied by an increase in the ordered peak (90°), which is consistent with the previous analysis.

The analysis shows that $\rho = 0.64$ is a transition point not only for the jamming and non-jamming states but also for the amorphous (random packing) and crystalline (ordered packing) states. However, the jamming density of 0.64 for random packing has not been rigorously proven.Fig. 3(b) and (c) show that even ρ is higher than 0.64, the jamming structure of (120°, 180°) still exists. Additionally, Fig. 3(a) shows that, for the (120°, 180°) jamming structure, it is possible to fill the gaps without disturbing the original positions of the jamming particles, thus making the calculation of the jamming angle ineffective. If this filling scheme is feasible, it is possible that the packing density will increase by further eliminating the (120°, 180°) jamming structures in the random system, leading to a series of random jamming densities (Jin & Yoshino, 2021; Parisi & Zamponi, 2010) without the appearance of ordered features. However, it is also possible that the presence of the (120°, 180°) jamming angles is inevitable in random packing due to the limitations of spherical geometry. For example, Q_6 increases with ρ in others' work (Jin & Yoshino, 2021), suggesting that the jamming structure of $\rho = 0.68$ under cyclic shear may be locally ordered. Therefore, further research is needed for the robust definition and calculation of the random jamming density, and this work provides an effective structural analysis method and a feasible direction for such investigations.

4. Conclusions

In summary, the jamming characteristics of packing structures with ρ ranging from 0.5 to 0.74 are analyzed from the perspective of the mechanical stability of packing structures generated from the DEM simulations. The developed free particles identification method is used to verify the transition point of $\rho = 0.64$ as a turning point of the jamming characteristics. It confirms the random jamming characteristics of the RCP structure and shows the gradual disappearance of the free volume with ρ. Based on this method, a jamming angle analysis is proposed which can identify both random and ordered structures, suggesting that further densification of the RCP structure requires a corresponding ordering transition. J_{90} can serve as an ideal order parameter for equal hard sphere packing systems, providing a quantitative characterization

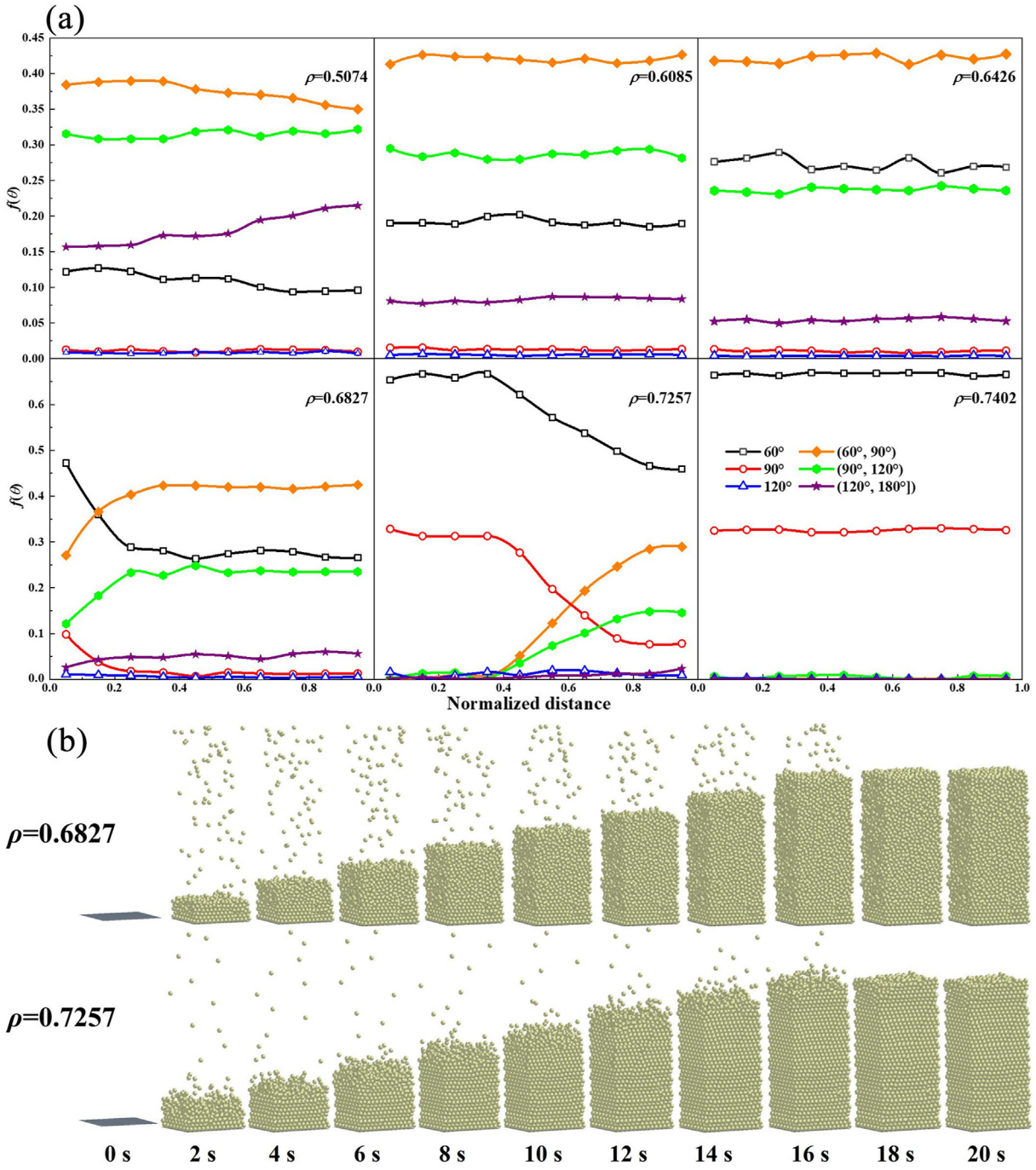

Fig. 8. (a) Relationship between $f(\theta)$ and normalized boundary distance for different jamming angles in various packings, where the packings are equally divided into ten layers according to the distance from the particles to the bottom of the container, and the probabilities of jamming angles within different layers are calculated. (b) Evolution of packing structure with time for $\rho = 0.6827$ and $\rho = 0.7257$.

of the degree of the order/randomness of a packing structure. Furthermore, the analyses on the evolution of the jamming angle with ρ and the correlation between the jamming angles explain that a random particle packing cannot transit from RCP to an ordered dense packing by successively increasing the density is due to the large presence of metastable jamming of (60°, 90°). Our approach and results identify a unique structural feature/correlation of order-jamming-metastable states, which has important implications for exploring a fully microscopic theory of the glass state as well as the design of amorphous materials and related composites.

CRediT authorship contribution statement

Wei Fan: Writing – original draft, Visualization, Software, Investigation, Formal analysis, Conceptualization. **Ju Wang:** Writing – review & editing, Methodology, Investigation, Formal analysis. **Xizhong An:** Writing – review & editing, Supervision, Methodology, Funding acquisition, Data curation, Conceptualization. **Yongli Wu:** Writing – review & editing, Software, Formal analysis. **Yi Zou:** Writing – review & editing, Software, Formal analysis. **Kejun Dong:** Writing – review & editing, Methodology, Data curation. **Runyu Yang:** Writing – review & editing,

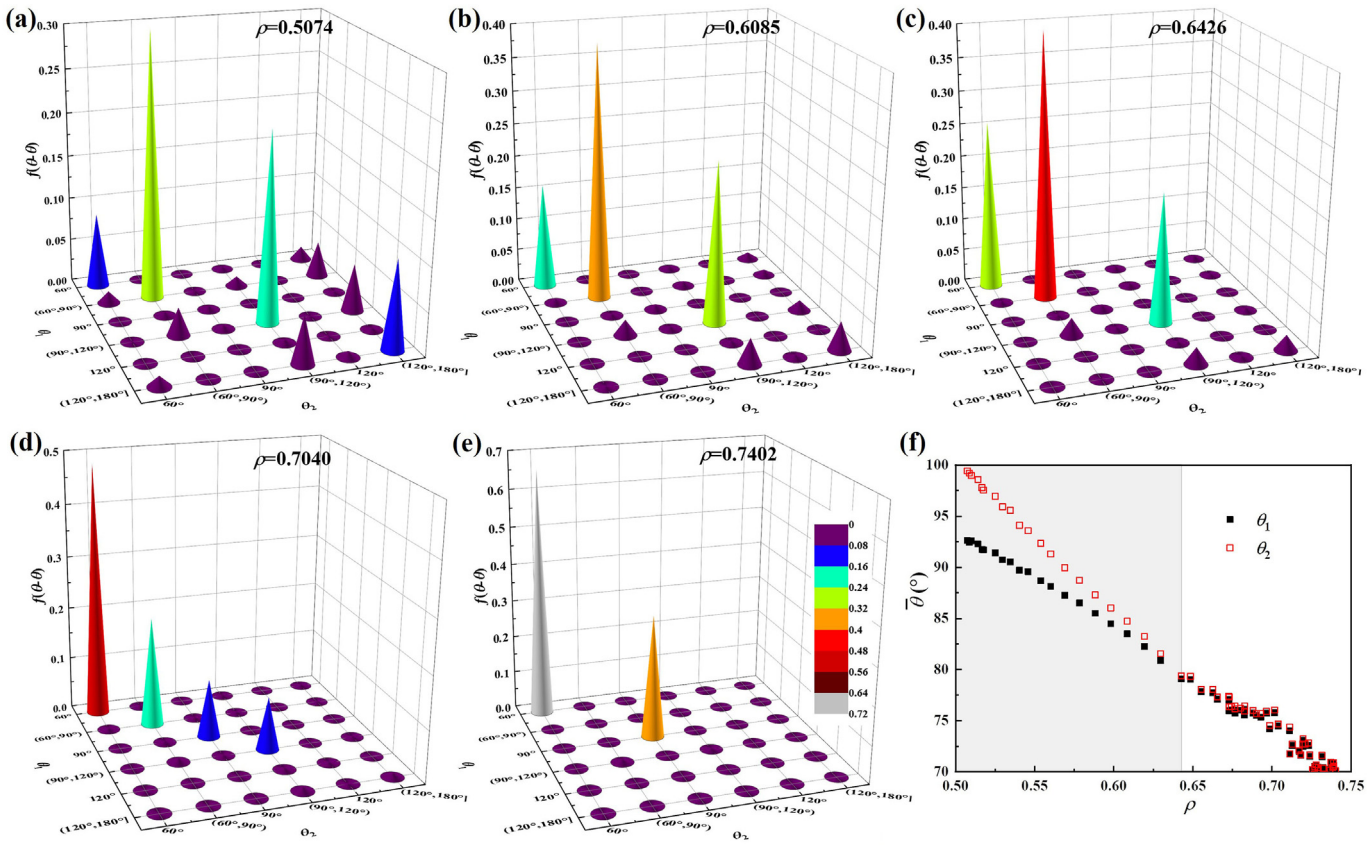

Fig. 9. (a)–(e) Probabilities of different jamming-jamming relations for different packings. (f) Relationship between average jamming angle and packing density.

Methodology, Data curation. **Ruiping Zou:** Writing – review & editing. **Aibing Yu:** Writing – review & editing.

Declaration of competing interest

The authors declare that they have no known competing financial interests or personal relationships that could have appeared to influence the work reported in this paper.

Acknowledgements

The authors are grateful to the National Natural Science Foundation of China (grant No. 51374070), Liaoning Revitalization Talents Program (grant No. XLYC1805007) of China, and Natural Science Foundation of Jiangsu Province (grant No. BK20200269) for the financial support to this work.

References

Amirifar, R., Dong, K., Zeng, Q., & An, X. (2018). Self-assembly of granular spheres under one-dimensional vibration. *Soft Matter, 14*(48), 9856–9869. https://doi.org/10.1039/C8SM01763H

Amirifar, R., Dong, K., Zeng, Q., An, X., & Yu, A. (2021). Effect of vibration mode on self-assembly of granular spheres under three-dimensional vibration. *Powder Technology, 380*, 47–58. https://doi.org/10.1016/j.powtec.2020.11.036

An, X. Z., Yang, R. Y., Dong, K. J., Zou, R. P., & Yu, A. B. (2005). Micromechanical simulation and analysis of one-dimensional vibratory sphere packing. *Physical Review Letters, 95*(20), Article 205502. https://doi.org/10.1103/PhysRevLett.95.205502

Anikeenko, A. V., & Medvedev, N. N. (2007). Polytetrahedral nature of the dense disordered packings of hard spheres. *Physical Review Letters, 98*(23), Article 235504. https://doi.org/10.1103/PhysRevLett.98.235504

Aste, T., & Weaire, D. L. (2000). *The pursuit of perfect packing*. Institute of Physics Pub.

Bernal, J. D. (1959). A geometrical approach to the structure of liquids. *Nature, 183*, 141–147. https://doi.org/10.1038/183141a0

Bernal, J. D. (1960). Geometry of the structure of monatomic liquids. *Nature, 185*, 68–70. https://doi.org/10.1038/185068a0

Bernal, J. D., & Mason, J. (1960). Packing of spheres: Co-Ordination of randomly packed spheres. *Nature, 188*, 910–911. https://doi.org/10.1038/188910a0

Binder, K. (1987). Theory of first-order phase transitions. *Reports on Progress in Physics, 50*(7), 783–859. https://doi.org/10.1088/0034-4885/50/7/001

Cohen, M. H., & Turnbull, D. (1964). Metastability of amorphous structures. *Nature, 203*(4948). https://doi.org/10.1038/203964a0, 964–964.

Dong, K. J., Yang, R. Y., Zou, R. P., An, X. Z., & Yu, A. B. (2009). Critical states and phase diagram in the packing of uniform spheres. *EPL (Europhysics Letters), 86*(4), Article 46003. https://doi.org/10.1209/0295-5075/86/46003

Fan, W., Gou, D., Liu, X., Li, M., An, X., Dong, K., Zou, R., Zhang, H., Fu, H., Yang, X., & Zou, Q. (2022). Air impact induced densest amorphous granular materials: Formation, dynamics, and mechanisms. *Physical Review B, 105*(2), Article L020202. https://doi.org/10.1103/PhysRevB.105.L020202

Finney, J. L. (1970). Random packings and the structure of simple liquids. I. The geometry of random close packing. *Proceedings of the Royal Society of London - Series A: Mathematical and Physical Sciences, 319*(1539), 479–493. https://doi.org/10.1098/rspa.1970.0189

Gou, D., An, X., Yang, X., Fu, H., & Zhang, H. (2017). CFD-DEM modeling on air impact densification of equal spheres: Structure evolution, dynamics, and mechanism. *Powder Technology, 322*, 177–184. https://doi.org/10.1016/j.powtec.2017.09.019

Hales, T. C. (2006). Historical overview of the kepler conjecture. *Discrete & Computational Geometry, 36*(1), 5–20. https://doi.org/10.1007/s00454-005-1210-2

Hoy, R. S. (2017). Jamming of semiflexible polymers. *Physical Review Letters, 118*(6), Article 068002. https://doi.org/10.1103/PhysRevLett.118.068002

Jin, Y., & Yoshino, H. (2021). A jamming plane of sphere packings. *Proceedings of the National Academy of Sciences of the United States of America, 118*, Article e2021794118. https://doi.org/10.1073/pnas.2021794118

Johnson, W. L. (1999). Bulk glass-forming metallic alloys: Science and technology. *MRS Bulletin, 24*, 42–56. https://doi.org/10.1557/S0883769400053252

Kamien, R. D., & Liu, A. J. (2007). Why is random close packing reproducible? *Physical Review Letters, 99*(15), Article 155501. https://doi.org/10.1103/PhysRevLett.99.155501

Karayiannis, N. C., & Laso, M. (2008). Dense and nearly jammed random packings of freely jointed chains of tangent hard spheres. *Physical Review Letters, 100*, Article 050602. https://doi.org/10.1103/PhysRevLett.100.050602

Liu, L. (2003). Simulation of microstructural evolution during isostatic compaction of monosized spheres. *Journal of Physics D: Applied Physics, 36*(15), 1881–1889. https://doi.org/10.1088/0022-3727/36/15/320

Liu, L., Zhang, L., & Liao, S. (2010). Structural signature and contact force distributions in the simulated three-dimensional sphere packs subjected to uniaxial compression. *Science China Physics, Mechanics & Astronomy, 53*(5), 892–904. https://doi.org/10.1007/s11433-010-0191-1

Liu, L. F., Zhang, Z. P., & Yu, A. B. (1999). Dynamic simulation of the centripetal packing of mono-sized spheres. *Physica A, 268*, 433–453. https://doi.org/10.1016/S0378-4371(99)00106-5

Lohr, M. A., Alsayed, A. M., Chen, B. G., Zhang, Z., Kamien, R. D., & Yodh, A. G. (2010). Helical packings and phase transformations of soft spheres in cylinders. *Physical Review E, 81*(4), Article 040401. https://doi.org/10.1103/PhysRevE.81.040401

Lubachevsky, B. D., & Stillinger, F. H. (1990). Geometric properties of random disk packings. *Journal of Statistical Physics, 60*(5–6), 561–583. https://doi.org/10.1007/BF01025983

Miao, J., Ercius, P., & Billinge, S. J. L. (2016). Atomic electron tomography: 3D structures without crystals. *Science, 353*, Article aaf2157. https://doi.org/10.1126/science.aaf2157

Miyagawa, H., Hiwatari, Y., Bernu, B., & Hansen, J. P. (1988). Molecular dynamics study of binary soft-sphere mixtures: Jump motions of atoms in the glassy state. *The Journal of Chemical Physics, 88*(6), 3879–3886. https://doi.org/10.1063/1.453836

Mueth, D. M., Jaeger, H. M., & Nagel, S. R. (1998). Force distribution in a granular medium. *Physical Review E, 57*, 3164. https://doi.org/10.1103/PhysRevE.57.3164

Nelson, D. R., & Spaepen, F. (1989). Polytetrahedral order in condensed matter. *Solid State Physics, 42*, 1–90. https://doi.org/10.1016/S0081-1947(08)60079-X

O'Hern, C. S., Silbert, L. E., Liu, A. J., & Nagel, S. R. (2003). Jamming at zero temperature and zero applied stress: The epitome of disorder. *Physical Review E, 68*, Article 011306. https://doi.org/10.1103/PhysRevE.68.011306

Palombo, M., Gabrielli, A., Servedio, V. D. P., Ruocco, G., & Capuani, S. (2013). Structural disorder and anomalous diffusion in random packing of spheres. *Scientific Reports, 3*, 2631. https://doi.org/10.1038/srep02631

Parisi, G., Urbani, P., & Zamponi, F. (2020). *Theory of simple glasses: Exact solutions in infinite dimensions*. Cambridge University Press.

Parisi, G., & Zamponi, F. (2010). Mean-field theory of hard sphere glasses and jamming. *Reviews of Modern Physics, 82*(1), 789–845. https://doi.org/10.1103/RevModPhys.82.789

Schröder-Turk, G. E., Mickel, W., Schröter, M., Delaney, G. W., Saadatfar, M., Senden, T. J., Mecke, K., & Aste, T. (2010). Disordered spherical bead packs are anisotropic. *EPL (Europhysics Letters), 90*(3), Article 34001. https://doi.org/10.1209/0295-5075/90/34001

Scott, G. (1960). Packing of spheres: Packing of equal spheres. *Nature, 188*, 908–909. https://doi.org/10.1038/188908a0

Sheng, H. W., Luo, W. K., Alamgir, F. M., Bai, J. M., & Ma, E. (2006). Atomic packing and short-to-medium- range order in metallic glasses. *Nature, 439*, 419–425. https://doi.org/10.1038/nature04421

Steinhardt, P. J., Nelson, D. R., & Ronchetti, M. (1983). Bond-orientational order in liquids and glasses. *Physical Review B, 28*(2), 784–805. https://doi.org/10.1103/PhysRevB.28.784

Szpiro, G. (2003). *Kepler's conjecture: How some of the greatest minds in history helped solve one of the oldest math problems in the world*. John Wiley & Sons.

Tong, H., & Tanaka, H. (2018). Revealing hidden structural order controlling both fast and slow glassy dynamics in supercooled liquids. *Physical Review X, 8*(1), Article 011041. https://doi.org/10.1103/PhysRevX.8.011041

Tong, H., & Tanaka, H. (2019). Structural order as a genuine control parameter of dynamics in simple glass formers. *Nature Communications, 10*(1), 5596. https://doi.org/10.1038/s41467-019-13606-3

Torquato, S., Truskett, T. M., & Debenedetti, P. G. (2000). Is random close packing of spheres well defined? *Physical Review Letters, 84*(10), 2064–2067. https://doi.org/10.1103/PhysRevLett.84.2064

Wang, W. H. (2012). The elastic properties, elastic models and elastic perspectives of metallic glasses. *Progress in Materials Science, 57*, 487–656. https://doi.org/10.1016/j.pmatsci.2011.07.001

Wilken, S., Guerra, R. E., Levine, D., & Chaikin, P. M. (2021). Random close packing as a dynamical phase transition. *Physical Review Letters, 127*, Article 038002. https://doi.org/10.1103/PhysRevLett.127.038002

Yang, Y. (2021). Determining the three-dimensional atomic structure of an amorphous solid. *Nature, 592*, 60–64. https://doi.org/10.1038/s41586-021-03354-0

Yu, A. B., An, X. Z., Zou, R. P., Yang, R. Y., & Kendall, K. (2006). Self-assembly of particles for densest packing by mechanical vibration. *Physical Review Letters, 97*(26), Article 265501. https://doi.org/10.1103/PhysRevLett.97.265501

Zallen, R. (2008). *The physics of amorphous solids*. John Wiley & Sons.

Zhao, B., An, X., Zhao, H., Shen, L., Sun, X., & Zhou, Z. (2019). DEM simulation of the local ordering of tetrahedral granular matter. *Soft Matter, 15*(10), 2260–2268. https://doi.org/10.1039/C8SM02166J